

Acoustic skin effect with non-reciprocal Willis materials F

Cite as: Appl. Phys. Lett. **121**, 041701 (2022); <https://doi.org/10.1063/5.0093247>

Submitted: 27 March 2022 • Accepted: 10 June 2022 • Published Online: 27 July 2022

 Wen Cheng and  Gengkai Hu

COLLECTIONS

Paper published as part of the special topic on [Acoustic and Elastic Metamaterials and Metasurfaces](#)

F This paper was selected as Featured



View Online



Export Citation



CrossMark

ARTICLES YOU MAY BE INTERESTED IN

[An energy conserving mechanism for temporal metasurfaces](#)

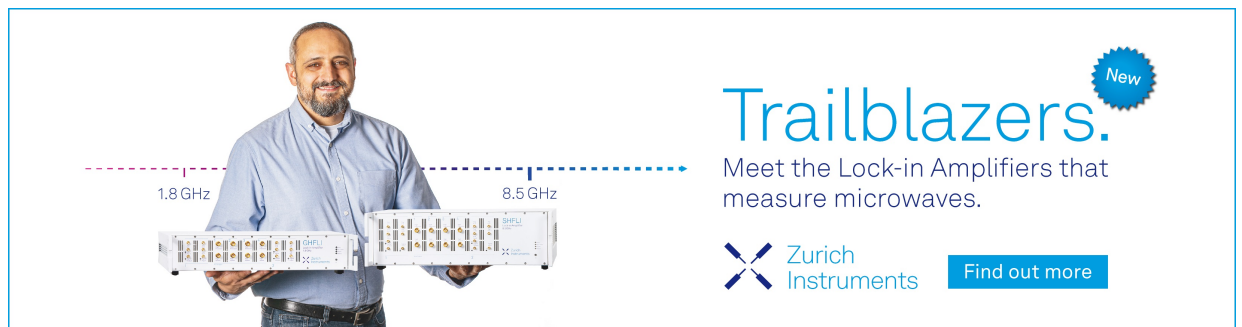
Applied Physics Letters **121**, 041702 (2022); <https://doi.org/10.1063/5.0097591>

[Acoustic energy harvesting metasurface based on surface wave conversion](#)

Applied Physics Letters **121**, 031701 (2022); <https://doi.org/10.1063/5.0097676>

[Tunable auxetic metamaterials for simultaneous attenuation of airborne sound and elastic vibrations in all directions](#)

Applied Physics Letters **121**, 081702 (2022); <https://doi.org/10.1063/5.0104266>



Trailblazers. New

Meet the Lock-in Amplifiers that measure microwaves.

 Zurich Instruments [Find out more](#)

Acoustic skin effect with non-reciprocal Willis materials

Cite as: Appl. Phys. Lett. **121**, 041701 (2022); doi: [10.1063/5.0093247](https://doi.org/10.1063/5.0093247)

Submitted: 27 March 2022 · Accepted: 10 June 2022 ·

Published Online: 27 July 2022



View Online



Export Citation



CrossMark

Wen Cheng  and Gengkai Hu^{a)} 

AFFILIATIONS

School of Aerospace Engineering, Beijing Institute of Technology, Beijing 100081, China

Note: This paper is part of the APL Special Collection on Acoustic and Elastic Metamaterials and Metasurfaces.

^{a)} Author to whom correspondence should be addressed: hugeng@bit.edu.cn

ABSTRACT

The Willis material model, coupling kinetic energy with a potential one, is shown to equip an extraordinary capacity in characterizing complex acoustic and elastic wave phenomena of metamaterials. This model has been further extended to active systems via breaking the symmetry between two coupling coefficients, leading to odd or non-reciprocal Willis material models [Quan *et al.*, Nat. Commun. **12**(1), 2615 (2021)]. In this work, through a 2D homogenous non-reciprocal acoustic Willis material (NRAWM), we demonstrate that the bulk local mode, referred to as skin effect in non-Hermitian systems, can survive on boundary of NRAWMs under proper conditions. The direction of the localization is closely related to the intrinsic direction embedded in the NRAWMs, and the localization is robust and topologically protected. To validate the prediction, a 2D discrete lattice made of non-local active acoustic scatterers is proposed and then homogenized as a NRAWM based on the retrieval method. The far-field radiation patterns of the local modes for both the 2D discrete lattice and the homogenized 2D NRAWM are evaluated, and they are in good agreement with each other. This work paves the way to design and explore the rich wave phenomena in non-Hermitian acoustic systems.

Published under an exclusive license by AIP Publishing. <https://doi.org/10.1063/5.0093247>

The Willis material model is a dynamic homogenization framework for composites² and allows to couple pressure with particle velocity as well as momentum density with bulk strain. This model can characterize complex acoustic and elastic wave phenomena out of reach of classical theory, e.g., independent control of transmission and reflection,³ perfect wavefront manipulation,⁴ and many others.⁵ For acoustic waves, this coupling originates from the interaction between monopole and dipole modes due to asymmetry of sub-wavelength microstructure.⁶ Due to restriction of reciprocity and passivity, the coupling coefficients should be imaginary and symmetric.⁷ In this case, the coupling coefficients indicate intrinsic directionality in materials, i.e., its sign indicates the asymmetry of microstructure in the 1D case.⁸ This peculiar property allows acoustic Willis materials to achieve the valley Hall topological insulator from intrinsic properties of the materials⁹ and many others.¹⁰ With the development of non-reciprocal and active acoustic devices,¹¹ the reciprocal Willis material model needs to be extended in order to characterize the exotic wave phenomena in non-Hermitian systems.¹² To this end, active acoustic Willis scatterers are proposed to design meta-surface¹³ with a capacity to control reflection and transmission separately, or asymmetric polarizabilities are introduced in the active elastic Willis materials model to

characterize independently transmission and reflection of flexural wave as well as non-reciprocity.¹⁴ These interesting works by modifying the coupling coefficients extended the Willis material model from passive systems to active ones. However, the current works are mainly focused on unidirectional cases, where the directionality of the Willis model depends only on the sign of the coupling coefficients. A similar phenomenon in elastic¹⁵ and flexural waves¹⁶ can also be characterized by the odd elastic material model in 1D case, and the relevant active devices are proposed by piezoelectric materials with feedback.^{1,14,17} However, until now, there is no general homogenized framework to predict this effect even for acoustic waves, particularly for 2D cases. In this work, we will examine a 2D acoustic wave localization problem with non-reciprocal acoustic Willis material (NRAWM), where the vector form of the coupling terms can be well illustrated. We demonstrate that the bulk acoustic wave can exponentially localize on the boundary of NRAWM under proper conditions, which is referred to as skin effect in non-Hermitian systems.^{18,19} The localization direction is closely related to the intrinsic direction embedded in the NRAWM, and this bulk wave localization phenomenon is also robust and topologically protected. These findings, based on a homogeneous NRAWM, are also validated by constructing a 2D discrete lattice

made of non-local acoustic scatterers. A 2D homogenization method based on the retrieval method is proposed to evaluate the material constants of NRAWM from the distribution and property of non-local acoustic scatterer lattice. The far-field radiation patterns of the 2D discrete square lattice are in agreement with the results based on the homogenized NRAWM. Our work provides a general framework to explore exotic wave phenomena in acoustic non-Hermitian systems.²⁰

For a linear Cauchy acoustic model, acoustic pressure depends only on bulk strain and momentum on particle velocity. However, this relationship should be modified to account for more complicated interactions between acoustic waves and material microstructures. To this end, Willis² proposed a more general constitutive relation with cross coupling between kinetic and potential energy, later named Willis materials. In frequency domain, the constitutive equations of acoustic Willis materials read

$$\begin{aligned} -p &= \kappa \varepsilon_v + \mathbf{S}_1 \cdot \mathbf{v}, \\ \boldsymbol{\mu} &= \mathbf{S}_2 \varepsilon_v + \boldsymbol{\rho} \cdot \mathbf{v}, \end{aligned} \quad (1)$$

where p , ε_v , \mathbf{v} , and $\boldsymbol{\mu}$ refer to pressure, bulk strain, particle velocity, and momentum, respectively, κ and $\boldsymbol{\rho}$ refer to bulk modulus and anisotropic mass density tensor, respectively. $\mathbf{S}_{1,2}$ are called Willis coupling coefficients. For simplification, we define two dimensionless parameters²¹ $\mathbf{W}_j = -i\mathbf{S}_j \cdot (\kappa\boldsymbol{\rho})^{-1/2} \{j = 1, 2, i^2 = -1\}$. The coupling terms $\mathbf{W}_{1,2}$ are vectors in 2D and 3D cases (scalars in 1D case). Reciprocity and passivity of the medium require that \mathbf{W}_1 and \mathbf{W}_2 should be equal and purely real vectors (the components of vector are all real) $\mathbf{W} = \mathbf{W}_1 = \mathbf{W}_2 \in \mathbb{R}^2$.⁷ If non-reciprocity and external energy exchange are allowed, these need $\mathbf{W}_1 \neq \mathbf{W}_2$, leading to NRAWM. In the following analysis, for simplification, we assume that $\mathbf{W}_{1,2}$ are real vectors, and the density tensor is isotropic ($\boldsymbol{\rho} = \rho\mathbf{I}$). These assumptions satisfy the necessary conditions of objectivity and causality, only time-reversal symmetry and passivity no longer hold. For complex coupling parameters ($\mathbf{W}_{1,2} \in \mathbb{C}^2$), discussions will be provided through some examples in the [supplementary material](#). While a plane time-harmonic wave ($p \propto e^{-ik_x x + i\omega t}$, ω is angular frequency) is assumed, with the help of Eq. (1) and the following geometric and equilibrium equations:

$$\begin{aligned} \nabla \cdot \mathbf{v} &= \dot{\varepsilon}_v, \\ -\nabla p &= \dot{\boldsymbol{\mu}}, \end{aligned} \quad (2)$$

we derive the dispersion relation of the homogeneous NRAWM as

$$\begin{aligned} (1 + \mathbf{W}_1 \cdot \mathbf{W}_2)k^2 - (\mathbf{k} \cdot \mathbf{W}_1)(\mathbf{k} \cdot \mathbf{W}_2) \\ + i(\mathbf{W}_2 - \mathbf{W}_1) \cdot \mathbf{k}\omega\sqrt{\rho/\kappa} - \frac{\omega^2\rho}{\kappa} = 0, \end{aligned} \quad (3)$$

with the wave vector $\mathbf{k} = k_x \mathbf{n}_x + k_y \mathbf{n}_y$ for 2D cases. Equation (3) implies that the spectrum of the homogeneous NRAWM may be complex when $\mathbf{W}_1 \neq \mathbf{W}_2$. For illustration purposes, we choose the following material constants $\boldsymbol{\rho} = \rho_0 \mathbf{I}$, $\kappa = \rho_0 c_0^2$ (as $\rho_0 = 1.013 \text{ kg/m}^3$, $c_0 = 340 \text{ m/s}$ are density and wave speed of air), and the spectra over Brillouin zone in ($k_x, k_y \in [-1, 1]$) are given in Fig. 1 with the different directions of $\mathbf{W}_{1,2}$ indicated by arrows. As it is shown, when $\mathbf{W}_1 \neq \mathbf{W}_2$, the directional parameters $\mathbf{W}_{1,2}$ have little effect on the real parts of the spectra [Figs. 1(a) and 1(d)]; however, they will have a significant influence on the imaginary parts of the spectra [Figs. 1(b) and

1(e)]. When $\mathbf{W}_1 = \mathbf{W}_2$, the medium becomes reciprocal, as also shown in Figs. 1(g) and 1(h), the imaginary part of the spectrum vanishes, as expected. If we predefine a path over Brillouin zone [e.g., as indicated by the inset in Fig. 1(c)] and plot the complex spectrum marked with arrows, it will show a unique non-Hermitian topological feature. For a homogeneous NRAWM, the Brillouin zone is unbounded [blue line in Figs. 1(c) and 1(f)]; however, a finite size material element with a given period will have the bounded Brillouin zone. Due to periodic conditions, the boundary of the Brillouin zone forms a loop [black line in Figs. 1(c) and 1(f)], and this makes the spectrum wraparound ω_0 . The spectra can trace out two non-degenerate arcs in the case of $\mathbf{W}_1 \neq \mathbf{W}_2$, contrary to the doubly degenerate reciprocal case [Fig. 1(i)], winding direction is determined by $\arg(\mathbf{W}_{1,2})$. Systems with such spectra will exhibit distinctive non-Hermitian topological features, referred to as the skin effect, which is a topological phenomenon in non-Hermitian systems characterized by topological invariant, i.e., the winding number.¹⁹ For a given wave vector along the direction θ , the winding number is calculated by $\nu_w(\theta) = \frac{1}{2\pi i} \int_{-R}^R \frac{\partial}{\partial k_r} \ln[\omega(k_r) - \omega_0] dk_r$, where k_r is the wave vector along the direction θ , R is the boundary of the Brillouin zone, and ω_0 is the excitation circular frequency. Based on argument principle,²² $\nu_w(\theta) \neq 0$ implies existence of non-trivial mode along the given direction θ [$\nu_w(\theta) = 1$] or opposite direction [$\nu_w(\theta) = -1$], and the localization region can be obtained by scanning all directions. In this case, the acoustic field will localize on the boundary of the medium, no matter the location of source. To calculate the winding number for the homogeneous NRAWM, we should replace the integral range by $-R < k_r < R$, while taking $R \rightarrow \infty$. Within the proposed framework of NRAWM, the localization of acoustic pressure can be designed by tailoring the angles of two coupling coefficient vectors. To illustrate this idea, we plot in Fig. 2 the winding number contours as a function of the intrinsic directionality $\arg(\mathbf{W}_{1,2})$ and the localization angle θ . For convenience, in the plot, we fixed $\arg(\mathbf{W}_1)$, indicated by the black arrow in the figure, and only changed $\arg(\mathbf{W}_2)$.

As shown in Fig. 2, the non-trivial mode can always be excited in NRAWMs, except for reciprocal case [$\arg(\mathbf{W}_1) = \arg(\mathbf{W}_2)$], and the localization angle is sensitive to the intrinsic direction in the NRAWM. For example, if we fix $\arg(\mathbf{W}_{1,2})$, the localization region can be determined by the interception of the horizontal line of a given $\arg(\mathbf{W}_2)$ with the red region [e.g., black dashed line in Fig. 2(a)]. For a better illustration, we present in Fig. 3 the numerical simulations on the acoustic skin effect with various combinations of \mathbf{W}_1 and \mathbf{W}_2 . In the computation, as it is shown in Fig. 3(a), the outside region is the Cauchy acoustic medium with $\rho_0 = 1.013 \text{ kg/m}^3$, $c_0 = 340 \text{ m/s}$, and the NRAWM forms—a region with charcoal gray, and the material constants of the NRAWM are $\boldsymbol{\rho} = \rho_0 \mathbf{I}$ and $\kappa = \rho_0 c_0^2$. For a better comparison of the localization direction, we apply monopole sources (yellow sign) with same flux density at the center of the NRAWM. The acoustic module of COMSOL Multiphysics is used for computation, and the proposed model is incorporated in a weak form. The results are shown, respectively, in Figs. 3(b)–3(d) for pressure fields with three different relations of $\arg(\mathbf{W}_{1,2})$; here, we fix $\arg(\mathbf{W}_1) = \pi/4$, and $\arg(\mathbf{W}_2)$ are taken $\pi/2$, 0 , and $\pi/4$, respectively. The far-field radiation patterns [along the dashed line in Fig. 3(a)] are also given in Figs. 3(b)–3(d) in a polar diagram. It is easy to check that the computed localization regions are in line with the predictions based on Fig. 2 (the angle where $\nu_w = 1$ are shown in Fig. 3 with gray sector), indicating that the acoustic pressure localization region is determined by

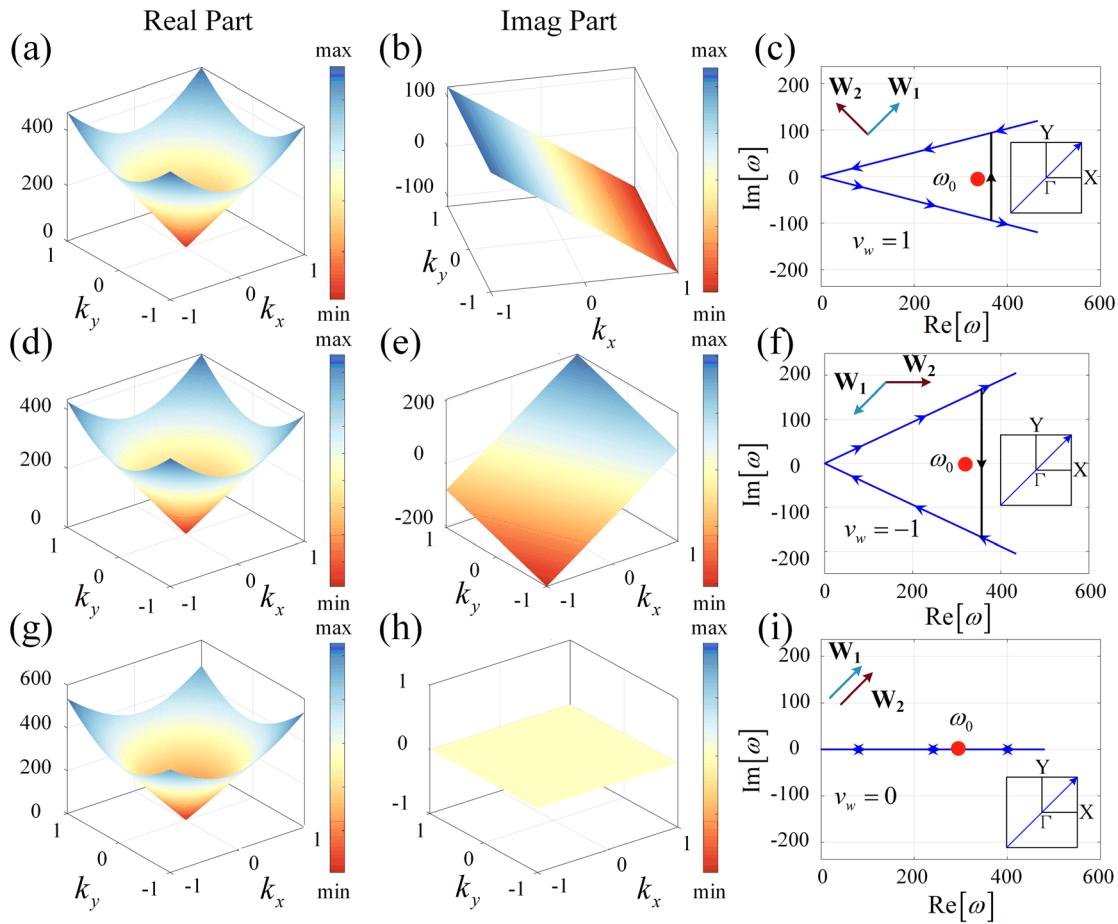


FIG. 1. Complex dispersion with different relations of coupling vectors. (a), (d), and (g) The corresponding real part of the spectra. (b), (e), and (h) The imaginary ones. The norms of the coupling vectors $|\mathbf{W}_{1,2}|$ are both 0.5, and the directions are indicated by corresponding arrows in (c), (f), and (i). The spectra are shown in (c), (f), and (i) for evaluating topological invariant ν_w , and the blue arrows indicate the direction of increasing \mathbf{k} .

topological invariant. It seems that a linear correlation between localization direction and $\arg(\mathbf{W}_1 - \mathbf{W}_2)$ may exist; however, proving this claim needs a further study. In contrast, there is no localized pressure field for the reciprocal acoustic Willis medium [$\arg(\mathbf{W}_{1,2}) = \pi/4$], as

indicated in Figs. 3(d) and 3(g). It should be mentioned that even though the winding number is 0, the scattered pattern is not a perfect circle, caused probably by cross coupling between monopole and dipole radiations.²¹ If the position of monopole source is changed, the

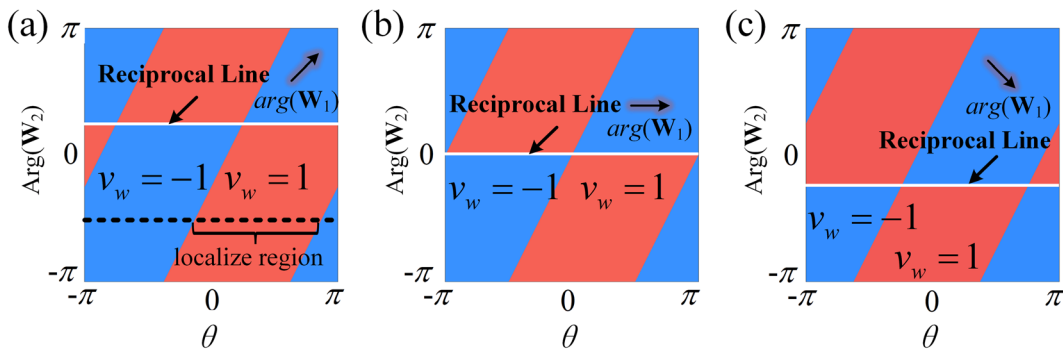


FIG. 2. Winding number contour as a function of $\arg(\mathbf{W}_2)$ and localization angle θ while $\arg(\mathbf{W}_1)$ is fixed, $\arg(\mathbf{W}_1) = \pi/4$ (a), 0 (b), and $-\pi/4$ (c). The white lines in each figure represent the case of $\arg(\mathbf{W}_1) = \arg(\mathbf{W}_2)$, i.e., reciprocal case, so the winding number is 0. The norms of coupling vectors are both 0.5, and the direction of \mathbf{W}_1 is indicated by black arrows.

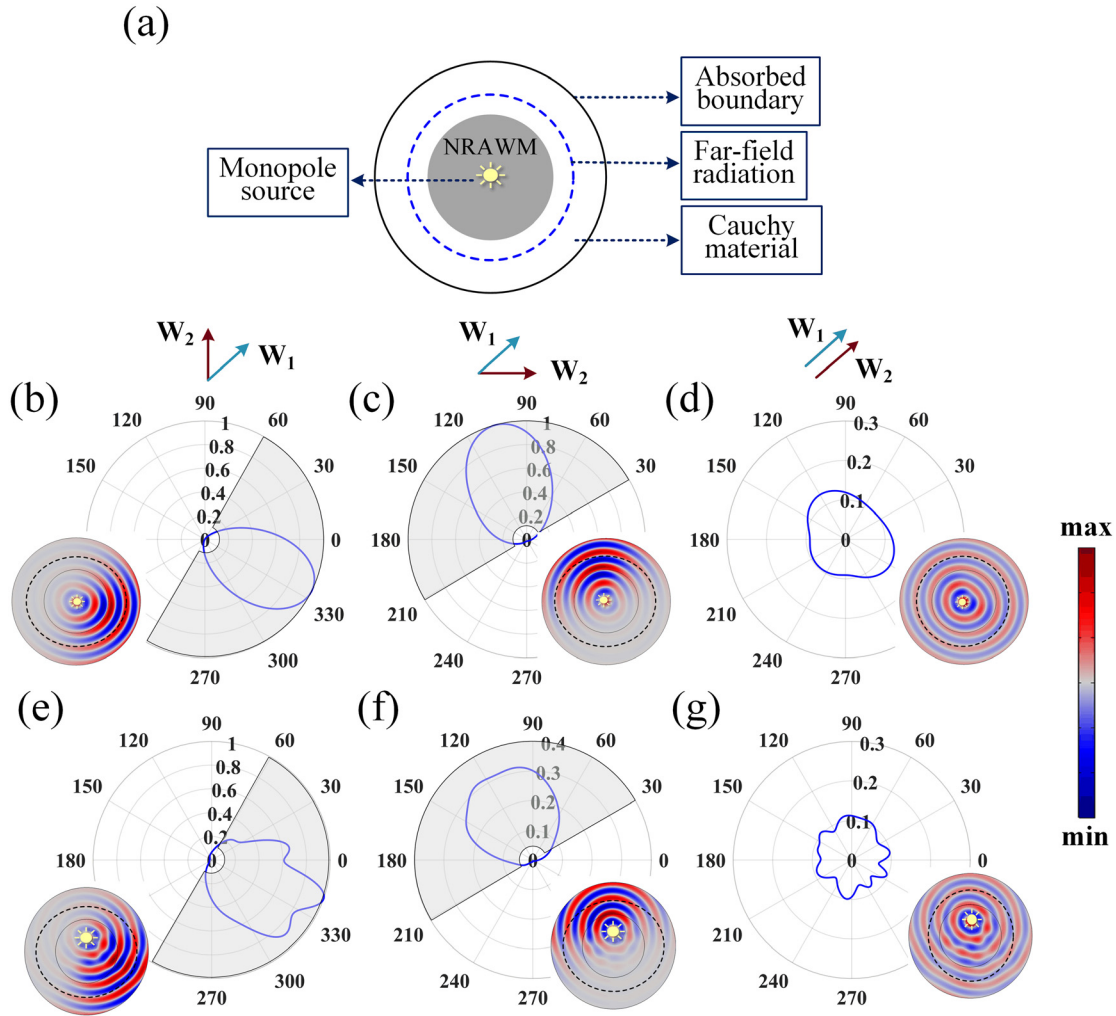


FIG. 3. Simulations on the acoustic pressure field with different relations between W_1 and W_2 for a homogeneous NRAWM. (a) The sketch of the calculation model. (b) and (c) Acoustic pressure localization (skin effect) and the far-field radiation patterns on dash circle lines when $W_1 \neq W_2$. (e) and (f) Influence of source position [with polar coordinates $(0.4, \pi/2)$] in NRAWMs. (d) and (g) The reciprocal case $W_1 = W_2$ for comparison. All the results are normalized by the max pressure in (b).

localization directions will not be significantly altered with the NRAWMs, but not so for the reciprocal Willis acoustic model, as shown in Figs. 3(e)–3(g). As a result, the localization is robust with source disturbance with the NRAWMs.²³

Theoretically, the local acoustic mode could appear on the boundary of the homogenous NRAWM, and the localization direction was determined by the intrinsic direction in the material. To validate the theoretical findings, particularly by experiment, a practical realization of the homogenous NRAWM must be at hand. To this end, we will use non-local acoustic scatterer lattice to mimic a homogenous NRAWM. The non-local acoustic scatterer is an active acoustic device with both loudspeaker and the acoustic sensor, the sensor detects local pressure as a signal, and the loudspeaker exports it with a pre-defined amplification. The similar acoustic device has been used in non-reciprocal acoustic transmission in the 1D case.^{12,24} Here, we will extend the concept to 2D case and more importantly establish its

connection with NRAWM. Figure 4(a) illustrates the proposed model of a square lattice made of non-local acoustic scatterers. The considered wavelength is assumed much longer than the scatterer, so the speaker can be considered as a point source (monopole). Speaker (red square) and sensor (blue square) are located along a circle with radius R_s , as shown in the enlarged view, and the length of the cell is denoted by $L_c (>2R_s)$. To reduce interference between the sources and other scatterers, the size of the unit cell should be carefully evaluated. For a single scatterer located in free space, the governing equation can be written as follows:

$$\nabla^2 p + |k|^2 p = Gp(\mathbf{x}_s)\delta(\mathbf{x} - \mathbf{x}_m), \quad (4)$$

where \mathbf{x}_m and \mathbf{x}_s indicate the locations of monopole source and sensor, respectively, \mathbf{k} represents wave vector, and δ denotes Dirac function of a 2D space, which is 1 in the origin and 0 otherwise. The right-hand side of Eq. (4) results from external source excitation, and G

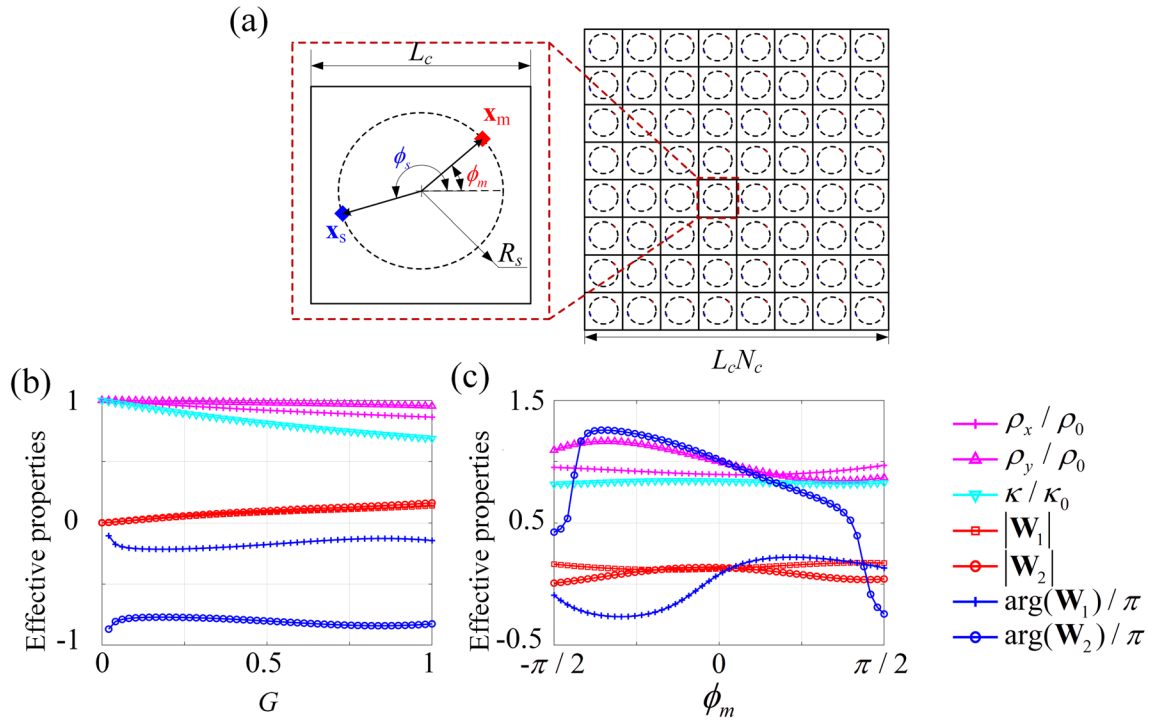


FIG. 4. (a) The sketch of non-local acoustic scatterer of length L_c and its $N_c \times N_c$ square lattice. \mathbf{x}_m and \mathbf{x}_s are the coordinates of the monopole source (loudspeaker) and sensor, respectively. ϕ_m and ϕ_s denote the geometric angle of monopole source and sensor, respectively. (b) and (c) Homogenized material constants at 800 Hz. (b) Effective material parameters as a function of gain factor G , the geometric angles are fixed as $\phi_m = \pi/4$ and $\phi_s = 3\pi/4$, and (c) effective material parameters as a function of geometry angle ϕ_m in which $G = 0.5$ and $\phi_s = \pi$. The geometric parameters are set as $L_c = 0.1$ m and $R_s = 0.045$ m.

means the acoustic pressure gain of the active scatterer. With the basic solution of Helmholtz equation in a 2D case, the scattered field generated by the monopole mode can be expressed as $p_m(\mathbf{x}) = iGp(\mathbf{x}_s)H_0^{(1)}(k(\mathbf{x} - \mathbf{x}_m))/4$, where $H_0^{(1)}$ is the zero-order Hankel function of the first kind. The non-local scatterer with additional artificial actuator can bring in asymmetric coupling between two acoustic polarization fields, and this will generate an NRAWM with $\mathbf{W}_1 \neq \mathbf{W}_2$. Furthermore, as the actuator in the scatterer only works with energy injection, this will also bring in non-Hermitian effect to the system. Interestingly, this active scatterer also has two geometric directions (ϕ_m for \mathbf{x}_m and ϕ_s for \mathbf{x}_s) as shown in Fig. 4(a), which can be characterized by previously examined NRAWM. So, in the following, we will homogenize the square lattice made of the non-local acoustic scatterers as a NRAWM and will use the retrieval method²⁵ to derive its homogenized material constants. More details can be found in the [supplementary material](#); here, we give directly the homogenization results in Figs. 4(b) and 4(c).

In a long wave approximation (800 Hz), the effective properties of the non-local scatterer lattice depend on ϕ_m and ϕ_s , and the gain factor G . For a passive case, i.e., $G \rightarrow 0$, the effective properties are the same as the background material, $\rho_{eff} = \rho_0 \mathbf{I}$, $\kappa_{eff} = \rho_0 c_0^2$, and $\mathbf{W}_1 = \mathbf{W}_2 = \mathbf{0}$. However, for a general case, whereas $G \neq 0$, the angles ϕ_m and ϕ_s generally monitor the two intrinsic directions $\arg(\mathbf{W}_{1,2})$ of the NRAWM, and the gain factor G contributes to the amplitudes of $\mathbf{W}_{1,2}$. With these connections between the non-local scatterer lattice and the homogenized NRAWM, we are ready to construct the local

mode predicted by a NRAWM with the non-local scatterer lattice by just tailoring the parameters ϕ_m and ϕ_s . It is worth noting that the effective density is not isotropic; however, this anisotropy is small and has less influence on the localization direction compared with two coupling vectors. For these reasons, we discarded the anisotropy in density to better illustrate the effect of coupling terms.

It should be mentioned that the radius R_s will affect quality of the localized patterns, but not the physical phenomenon (pressure localization) itself. The choice of R_s is subjected to two conditions. First, it will be large enough to avoid self-excitation. Second, the dilute condition for the homogenization method must be met (since dilute solution is adopted). Combining these two conditions, we set $R_s = 0.045$ m in our model. The simulation results on the acoustic skin effect by the homogenized NRAWM and by the active scatterer lattice are both illustrated in Fig. 5. The sources with the same flux density are located in the origin, and a square lattice with 10×10 cells is placed in an acoustic fluid. As discussed above, the direction of localized acoustic waves is tailored by the intrinsic directions of $\mathbf{W}_{1,2}$, which are realized by adjusting the geometric angle $\phi_{m,s}$ of the active scatterer lattice. The computed results with the homogenized NRAWM and its corresponding lattice are shown, respectively, in Figs. 5(a) and 5(b) for the localization direction 0, and in Figs. 5(d) and 5(e) for the localization direction $\pi/4$. It can be seen that both models predicted almost the same skin effect appeared on the boundary. The patterns of far-field radiation along the black dash circle lines are also plotted in a polar system, as shown in Figs. 5(c) and 5(f), a good agreement of both

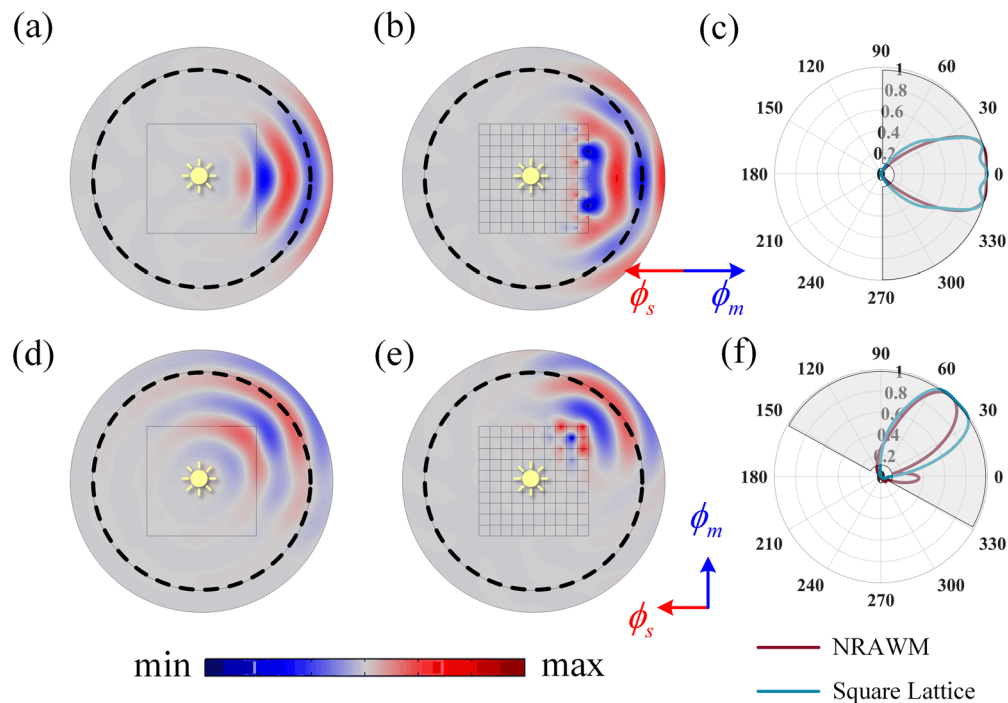


FIG. 5. Acoustic skin effect predicted by homogenized NRAWM and active scatterer lattice, and the corresponding far-field radiation patterns. A square of NRAWM and $2D$ 10×10 lattice ($R_s = 0.045$ m) with the same length of 1 m are placed in air-fluid. The intrinsic directions of homogenized NRAWM and two angles ϕ_m and ϕ_s of the scatterer are plotted with blue and red arrows, respectively. (a) and (b) Skin effect with localization angle 0; (d) and (e) skin effect with localization angle $\pi/4$. (c) and (f) Far-field radiation patterns of NRAWM and active scatterer lattice along with the dash circles in (a) and (b) and (d) and (e).

models is also observed, except for some discrepancies due to the non-uniform corner edge in the square lattice. These discrepancies may come from different aspects of our model: first, the point source will induce a singularity at origin, and this will affect the pressure distribution in the near field. Second, wave interference at the corner of the square lattice can take place, and its characterization by the two models may lead to discrepancy. Complex coupling terms can appear in the effective material model, and this can lead to a narrower localized pattern (as shown in the [supplementary material](#)). These results demonstrate that the proposed homogenization method is valid for designing the acoustic skin effect.

In summary, we predict the acoustic skin effect in a homogeneous NRAWM and demonstrate that it can also be achieved by an active scatterer lattice. Two internal directions of the homogeneous NRAWM determine the localization region of acoustic waves. To achieve NRAWM and tailor the internal directions, non-local acoustic scatterer lattice can be used and homogenized as NRAWM by the retrieval method. We demonstrate that the two geometric angles of sensor and monopole source in the unit cell correlate perfectly with two coupling vectors in the homogenized NRAWM, and they also monitor the energy exchange of the system. The predicted localization directions and far-field radiation patterns are in agreement with the lattice model and homogenized one, validating the proposed homogenization method. This proposed method can provide a general tool to investigate acoustic waves in non-Hermitian systems.

See the [supplementary material](#) for the complex Willis coupling terms and a detailed process of the retrieval method.

We thank the National Natural Science Foundation of China for their support (Grant Nos. 11632003, 11972083, and 11991030).

AUTHOR DECLARATIONS

Conflict of Interest

The authors have no conflicts to disclose.

Ethics Approval

Ethics approval is not required.

DATA AVAILABILITY

The data that support the findings of this study are available from the corresponding author upon reasonable request.

REFERENCES

- ¹L. Quan, S. Yves, Y. Peng, H. Esfahlani, and A. Alu, *Nat. Commun.* **12**(1), 2615 (2021).
- ²J. R. Willis, *Wave Motion* **3**(1), 1 (1981).
- ³J. Li, C. Shen, A. Diaz-Rubio, S. A. Tretyakov, and S. A. Cummer, *Nat. Commun.* **9**(1), 1342 (2018).
- ⁴G. W. Milton, M. Briane, and J. R. Willis, *New J. Phys.* **8**(10), 248 (2006).
- ⁵J. Yin, L. Cai, X. Fang, Y. Xiao, H. Yang, H. Zhang, J. Zhong, H. Zhao, D. Yu, and J. Wen, *Adv. Mech.* **52**(3), 1 (2022).
- ⁶C. F. Sieck, A. Alù, and M. R. Haberman, *Phys. Rev. B* **96**(10), 104303 (2017).

- ⁷M. B. Muhlestein, C. F. Sieck, A. Alu, and M. R. Haberman, *Proc. R. Soc. A* **472**(2194), 20160604 (2016).
- ⁸M. B. Muhlestein, C. F. Sieck, P. S. Wilson, and M. R. Haberman, *Nat. Commun.* **8**, 15625 (2017).
- ⁹H. Qu, X. Liu, and G. Hu, *Appl. Phys. Lett.* **119**(5), 051903 (2021).
- ¹⁰X. Su and D. Banerjee, *Phys. Rev. Res.* **3**(3), 033080 (2021).
- ¹¹C. Rasmussen, L. Quan, and A. Alù, *J. Appl. Phys.* **129**(21), 210903 (2021); J. Li, X. Wen, and P. Sheng, *ibid.* **129**(17), 171103 (2021).
- ¹²C. Cho, X. Wen, N. Park, and J. Li, *Commun. Phys.* **4**(1), 82 (2021).
- ¹³Y. Zhai, H. Kwon, and B. Popa, *Phys. Rev. B* **99**(22), 220301 (2019).
- ¹⁴Y. Chen, X. Li, G. Hu, M. R. Haberman, and G. Huang, *Nat. Commun.* **11**(1), 3681 (2020).
- ¹⁵M. Brandenbourger, X. Locsin, E. Lerner, and C. Coullais, *Nat. Commun.* **10**(1), 4608 (2019).
- ¹⁶Y. Chen, X. Li, C. Scheibner, V. Vitelli, and G. Huang, *Nat. Commun.* **12**(1), 5935 (2021).
- ¹⁷W. Cheng and G. Hu, *Sci. China Phys. Mech.* **64**(11), 1 (2021).
- ¹⁸L. Zhang, Y. Yang, Y. Ge, Y. Guan, Q. Chen, Q. Yan, F. Chen, R. Xi, Y. Li, and D. Jia, *Nat. Commun.* **12**(1), 6297 (2021); D. Zhou and J. Zhang, *Phys. Rev. Res.* **2**(2), 023173 (2020).
- ¹⁹J. Zhong, K. Wang, Y. Park, V. Asadchy, C. C. Wojcik, A. Dutt, and S. Fan, *Phys. Rev. B* **104**(12), 125416 (2021).
- ²⁰Y. Ashida, Z. Gong, and M. Ueda, *Adv. Phys.* **69**(3), 249 (2020).
- ²¹M. B. Muhlestein, B. M. Goldsberry, A. N. Norris, and M. R. Haberman, *Proc. R. Soc. A* **474**(2220), 20180571 (2018).
- ²²V. Bryant and A. F. Beardon, *Math. Gaz.* **63**(426), 278 (1979).
- ²³Y. Chen, Q. Zhang, Y. Zhang, B. Xia, X. Liu, X. Zhou, C. Chen, and G. Hu, *Adv. Mech.* **51**(2), 189 (2021).
- ²⁴N. Geib, A. Sasmal, Z. Wang, Y. Zhai, B. Popa, and K. Grosh, *Phys. Rev. B* **103**(16), 165427 (2021).
- ²⁵H. J. Lee, H. S. Lee, P. S. Ma, and Y. Y. Kim, *J. Appl. Phys.* **120**(10), 104902 (2016).